Available online at www.sciencedirect.com
SCIENCE DIRECT
Journal of Power Sources 148 (2005) 78–84
JOURNAL OF POWER SOURCES
www.elsevier.com/locate/jpowsour

# $LiCoO_2$ electrode/electrolyte interface of Li-ion rechargeable batteries investigated by in situ electrochemical impedance spectroscopy

Masayuki Itagaki [a,*], Nao Kobari [a], Sachiko Yotsuda [a], Kunihiro Watanabe [a], Shinichi Kinoshita [b], Makoto Ue [b]

[a] *Department of Pure and Applied Chemistry, Faculty of Science and Technology, Tokyo University of Science, Noda, Chiba 278-8510, Japan*
[b] *Mitsubishi Chemical Group, Science & Technology Research Center, 8-3-1, Chuo, Ami, Inashiki Ibaraki 300-0332, Japan*

Received 22 September 2004; received in revised form 14 January 2005; accepted 1 February 2005
Available online 22 March 2005

**Abstract**

An in situ electrochemical impedance spectroscopy was applied to the investigation of $LiCoO_2$ electrode in ethylene and ethyl methyl carbonates electrolyte. The electrode impedance was plotted on the three-dimensional diagram, which has real, imaginary and time axes, with the measurements of the charge (deintercalation) and discharge (intercalation) curves. The formation of the solid electrolyte interface (SEI) on $LiCoO_2$ electrode was discussed by the variation of impedance spectra. It was found that the SEI structure was constructed on $LiCoO_2$ electrode and its resistance changed by the reversible process. Moreover, the effects of vinylene carbonate and ethylene sulfite as additives into the electrolyte were investigated.


*Keywords:* Li-ion rechargeable battery; $LiCoO_2$; EIS; SEI; Vinylene carbonate; Ethylene sulfite

## 1. Introduction

The lithium-ion rechargeable batteries (LIRB) have been used for the power sources of the mobile electric devices instead of nickel–cadmium batteries recently. Great numbers of electrode materials and electrolytes have been developed from the expectation to evolve the LIRB. When the qualities of the electrode materials and electrolytes become higher, the precise controls of the electrode/electrolyte interfaces become more significant.

It is widely known that the stable film, which is called a solid electrolyte interface (SEI), is formed on the negative graphite electrode of LIRB [1–3]. The formation of SEI inhibits the decomposition of electrolyte on the negative electrode, and the SEI stabilizes the negative electrode. On the other hand, there are some papers concerning the SEI at the positive electrode/electrolyte interface. Aurbach et al. [4,5] reported the presence of SEI on $LiNiO_2$ electrode on basis of the measurements by a Fourier transformation infrared ray spectroscopy (FT-IR), a Raman spectroscopy, a X-ray photoelectron spectroscopy (XPS), a scanning electron microscope (SEM) and an electrochemical impedance spectroscopy (EIS). Ostrovskii et al. [6] confirmed the SEI on $LiNi_yCo_{(1-y)}O_2$ positive electrode by FT-IR and Raman spectroscopy, and revealed that several types of surface reactions occur depending on the type of electrolyte solutions. Zhang et al. [7] reported in various electrochemical methods involving EIS that the irreversible capacity of $LiNiO_2$ electrode in first cycle charge concerned with the change of the electrode structure and the reaction with the electrolyte.

The addition of the additives into the electrolyte influences the electrode/electrolyte interface. For example, it is known that the vinylene carbonate (VC) is effective additive to stabilize the negative graphite electrode [8–12]. Beside Aurbach et al. [11] investigated the influence of VC on the

* Corresponding author. Tel.: +81 4 7122 9492; fax: +81 4 7123 9890.
*E-mail address:* itagaki@rs.noda.tus.ac.jp (M. Itagaki).

0378-7753/$ – see front matter © 2005 Elsevier B.V. All rights reserved.
doi:10.1016/j.jpowsour.2005.02.007

reactions of $LiMn_2O_4$ and $LiNiO_2$ positive electrodes by a cyclic voltammetry (CV), chronopotentiometry, EIS, FT-IR, XPS, electrochemical quartz crystal microbalance (EQCM), and reported that the addition of VC decreased the interfacial impedance of the positive electrodes. As revealed in this paper [11], the investigation of the effect of the additive on positive electrode/electrolyte interface will be important subject for the development of LIRB. Furthermore recently, the ethylene sulfite (ES) is expected for the additive to form SEI film on the negative electrode. Wrodnigg et al. [13] reported the formation of SEI film on the negative electrode in propylene carbonate (PC) containing ES by CV and an Auger electron spectroscopy. Ota et al. [14] analyzed electrode surfaces in PC containing ES by a X-ray absorption fine structure (XAFS), a sulfur K-edge X-ray absorption near-edge structure spectroscopy (S K-edge XANES), XPS and a time-of flight-secondary ion mass spectrometry (TOF-SIMS), and reported that the organic film involving $Li_2SO_3$, R–$SO_3$Li, –C–S–C and –C–S–S–C– was formed on the negative electrode and the film involving $Li_2SO_4$ and sulfur was formed on the positive electrode. However, the effect of ES on the positive electrode/electrolyte interface during the charge and discharge cycle has not been clarified sufficiently.

Our group developed in situ electrochemical impedance spectroscopy (in situ EIS) by which impedance spectra can be determined simultaneously with the measurement of charge and discharge curves, and applied it to the analysis of SEI formation at negative electrode/electrolyte interface [10,15]. In the present paper, the in situ EIS is applied to the investigation of reactions on $LiCoO_2$, which is the typical material of the positive electrode, in ethylene carbonate (EC) + ethyl methyl carbonate (EMC) (3:7 by volume) electrolyte. The impedance parameters (a charge transfer resistance and a SEI resistance) are obtained by in situ EIS, and the variation of the electrode/electrolyte interface during the charge and discharge sequence is discussed. Moreover, the effects of additions of VC and ES into EC/EMC electrolyte on the electrode reactions are researched.

## 2. Experimental method

### 2.1. Electrodes and electrolyte

The electrochemical cell was same as one used in the previous paper [10]. The $LiCoO_2$ working electrode (WE) (1 cm × 0.4 cm, Mitsubishi Chemical Co.) was fabricated by pasting $LiCoO_2$ powder (27.5 mg $cm^{-2}$), carbon-conducting additive and a binder on aluminum foil. A lithium foil was used as the counter electrode (CE) and a lithium wire was used as the reference electrode (RE). A polyethylene separator was sandwiched between WE and CE. In order to prevent the deformation of WE due to the volume change by electrolysis, the WE and CE were fixed with aluminum and nickel plates, respectively. The electrolyte solutions were a mixture of an ethylene carbonate and an ethyl methyl carbonate (3:7 by volume), EC/EMC containing 2 wt% VC and EC/EMC containing 1 wt% ES. All electrolyte solutions contained 1 mol $dm^{-3}$ $LiPF_6$. All experiments were carried out at room temperature (25 °C) in a dry argon atmosphere.

### 2.2. Simultaneous measurements of charge–discharge curve and electrochemical impedance

The impedance spectra were measured successively by superimposing the small ac current on the dc current during the measurements of the charge–discharge curves. The dc current density was 0.2 mA $cm^{-2}$. The amplitude of the ac current was controlled to make the ac component of potential response smaller than 5 mV. The impedance measurement was performed in a frequency range from 10 mHz to 10 kHz, and started from high frequency toward low frequency in the logarithmic scan. In the present paper, the charge is defined as the deintercalation of lithium from the positive electrode, and the discharge is defined as the intercalation of lithium into the positive electrode. The experimental set-up consisted of a potentiostat (Hokuto Denko, HA501G) and a frequency response analyzer (FRA) (NF block, 5020) controlled by a personal computer (IBM, ThinkPad A22m) through GP–IB interface. The impedance spectra were measured successively during charge–discharge sequence, and plotted on the three-dimensional (3D) complex diagram that has a time axis. The plots were connected by the spline under tension function at each frequency. The cross-section of 3D impedance shell perpendicular to the time axis gives the instantaneous impedance at an arbitrary time [15]. The impedance and the parameters obtained by the impedance were represented by the values per the surface area (0.4 $cm^2$) of the working electrode.

### 2.3. Anodic polarization curves of platinum electrode in EC/EMC electrolyte

The working electrode was platinum wire whose diameter and length were 0.5 mm and 1 cm, respectively. CE and RE were lithium wires. The working electrode potential was scanned toward the anodic direction at 5 mV $s^{-1}$. The electrolyte solutions were same as those written in Section 2.1.

## 3. Results and discussion

### 3.1. Electrochemical measurements of $LiCoO_2$ electrode in EC/EMC (3:7 by volume ratio) involving 1 M $LiPF_6$

By the application of EIS to an analysis of electrode reaction, some time constants related to the surface structure can be discriminated. As the in situ EIS for secondary batteries, Osaka et al. [16] measured the impedance spectra of lithium electrode during charge–discharge sequence by superimposing ac to dc current, and analyzed the variation of impedance spectrum of lithium deposition. However, since the frequency range in the report [16] was from 10 Hz to 20 kHz, the data

regarding the charge transfer in the low frequency range could not be obtained in the case of lithium-ion rechargeable batteries. The properties of electrode/electrolyte interfaces should vary in the course of charge and discharge. Though the high frequency measurement in the impedance spectrum spends a short time, the relative long time is necessary to measure the low frequency components. Therefore, it is considered that the low frequency components in the impedance spectrum are deviated by the variation of electrode/electrolyte interface during charge–discharge sequence. Stoynov et al. proposed the compensation method for deviation of low frequency data by three-dimensional impedance plot [17], and applied it to the investigation of lead acid batteries [18]. Itagaki et al. [10] used this compensation method to analyze the electrochemical impedance of negative electrode in LIRB, and discussed the formation of SEI in the first charge. In the present paper, the above-mentioned in situ EIS is applied to the investigation of $LiCoO_2$ positive electrode/electrolyte interface in LIRB.

The 3D impedance diagram of $LiCoO_2$ positive electrode in EC/EMC electrolyte solution, which was measured simultaneously with the first charge, is shown in Fig. 1. The capacitive behavior is observed in the 3D impedance, and the diameter of the capacitive loop decreases with the charge time. As revealed in the previous papers [10,15], the cross-section of the 3D impedance shell, where the plots at each frequency were connected by the spline function, perpendicular

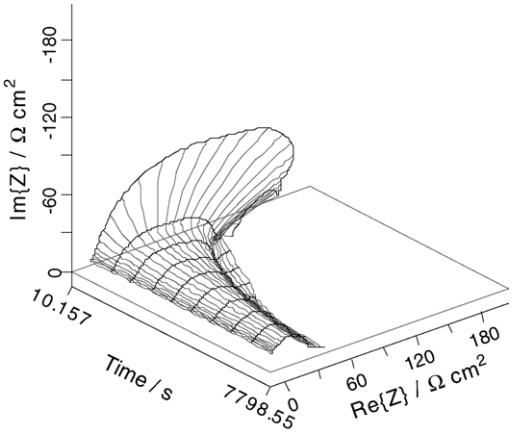


Fig. 1. Three-dimensional complex plots of electrochemical impedance of $LiCoO_2$ electrode in EC/EMC electrolyte solution during first charge.

to the time axis gives the instantaneous impedance. Fig. 2 shows the first cycle charge curve and the instantaneous impedance of $LiCoO_2$ electrode in EC/EMC electrolyte. In the charge curve, the potential attains to the plateau at 3.9 V and increases slightly until the potential where the charge completes. This feature of the charge curve is almost in agreement with those reported by Imanishi et al. [19] and Lee and Rhee [20]. The charge curve does not show the apparent potential plateau corresponding to the phase transition above 137 mAh $g^{-1}$ because the present electrode is assemblage

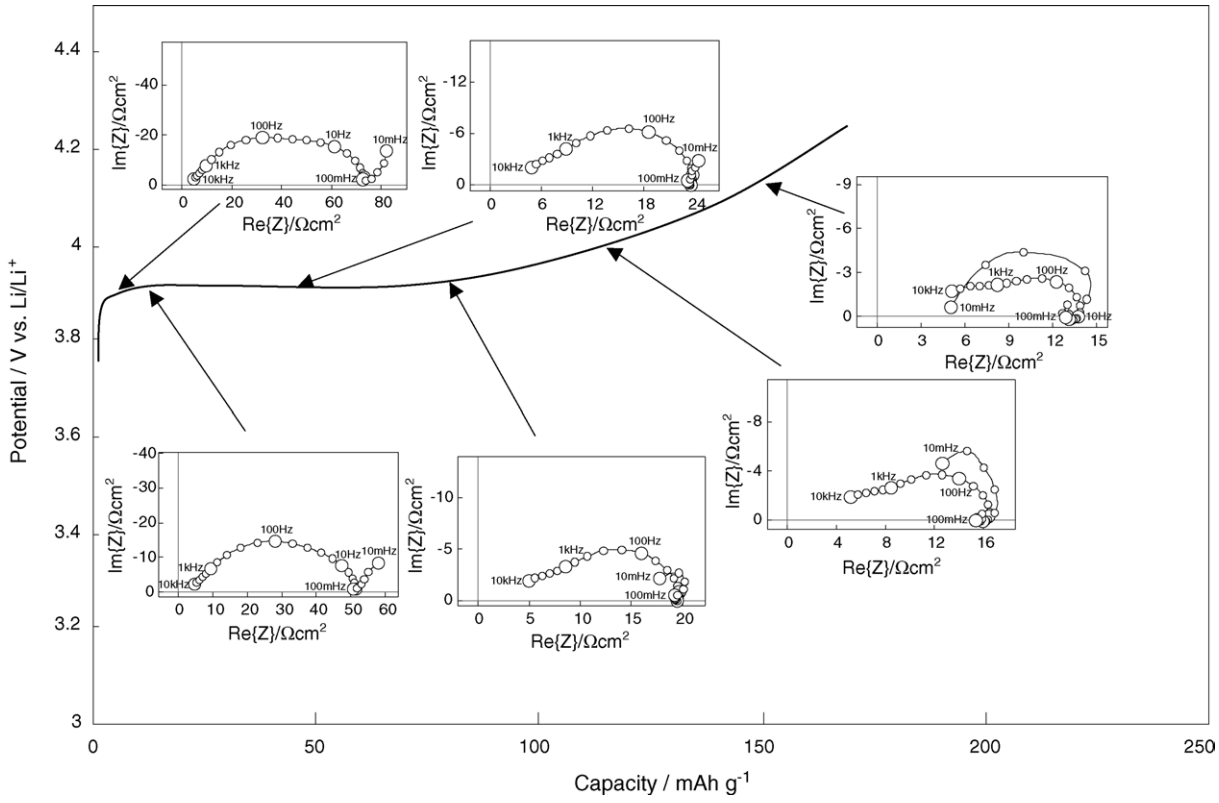


Fig. 2. Potential–capacity curve of the $LiCoO_2$ electrode in EC/EMC (3:7 by volume) containing 1 mol $dm^{-3}$ $LiPF_6$ in the first cycle charge and the complex plane plots of the instantaneous impedance. The dc current density is 0.2 mA $cm^{-2}$.

of the small oxide particles. The impedance at the initial period (10 mAh $g^{-1}$) describes the two capacitive loops in the frequency range between 100 mHz and 10 kHz and a part of diffusion impedance below 100 mHz. The capacitance of capacitive loop at the low frequency side could be estimated as an order of $10^{-3}$ F $cm^{-2}$. The electric double layer capacitance of plane electrode/electrolyte interface is an order of $10^{-5}$ F $cm^{-2}$ generally and the positive electrode has an actually huge surface area due to the porous structure. Therefore, it can be considered that the capacitive loop at low frequency side is related to the time constant of electric double layer capacitance and the charge transfer resistance on the particle of $LiCoO_2$. On the other hand, the capacitance of the capacitive loop at high frequency side is an order of $10^{-5}$ F $cm^{-2}$ and much smaller than electric double layer capacitance. Thus, the capacitive loop at high frequency side could be related to the time constant regarding SEI. Zhang et al. [7] studied the SEI formation on lithium nickel mixed oxide in the first charge and discharge cycle, and stated that high frequency loop was related to a parallel combination of SEI resistance and its capacitance. Since the electrode condition does not attain the equilibrium in the case of in situ EIS, the apparent diffusion Warburg impedance was not observed in the present analysis. At the potential nobler than 3.9 V, the negative resistance is observed in the impedance below 100 mHz. The negative resistance is often observed in the low frequency region, and related to the phenomenon that the electrode reaction rate decreases with the increase of the overvoltage generally. In this electrode system, the above-mentioned rate decrease may originate from the deep state of charge and/or the phase transition.

Aurbach et al. [4] measured the impedance of $LiCoO_2$ electrode in EC/dimethyl carbonate (DMC) at open-circuit voltage (OCV), and reported two capacitive loops. Since the diameter of the capacitive loop at high frequency side did not depend on the electrode potential, they [4] revealed that this loop was related to the Li-ion migration step through the film in the intercalation process. Jeong et al. [21] measured the impedance of $LiCoO_2$ electrode at various states of charge, and reported that the capacitive loop at high frequency side did not show the apparent potential dependence. Fey et al. [22] reported that the impedance spectra of $Li_xNi_yCo_{1-y}O_2$ in EC/diethyl carbonate (DEC) containing 1 M $LiPF_6$ consist of two depressed semicircles and that the high frequency loop did not depend on the intercalation level. Fey et al. [22] analyzed the impedance by the equivalent circuit involving the charge transfer resistance and the resistance associated with particle-to-particle contact among the oxide particles. On the other hand, Wu and Kim [23] measured the electrochemical impedance of $LiNi_{0.5}Mn_{1.5}O_4$ positive electrode, and reported that two capacitive loops and diffusion Warburg impedance were involved in the impedance. Furthermore, the diameters of the capacitive loops decrease with the potential in the paper by Wu and Kim [23]. Zhang et al. [7] observed one or two overlapped semicircles in complex impedance plots and the potential dependence in high frequency loop. In Fig. 2, the diameter of capacitive loop at high frequency side decreases with the charging time. In the above-mentioned papers [4,7,21–23], several capacitive loops were observed in the complex impedance plots of the positive electrode. However, the potential dependence and the interpretation of the high frequency loop have not agreed among them. In the present paper, in situ impedance is measured during the first charge and discharge cycle, and the SEI formation will be discussed by the variation of the high frequency loop in Section 3.3.

### 3.2. Charge and discharge curves of $LiCoO_2$ electrode in various electrolyte solutions

Fig. 3 shows the charge and discharge (potential–capacity) curves of $LiCoO_2$ electrode in three kinds of electrolyte solutions. The shape of the curves is almost same as the reported ones [19,20], and does not depend on the kind of electrolyte solutions. The coulombic efficiencies of first cycle in EC/EMC, EC/EMC with 2 wt% VC and EC/EMC with 1 wt% ES were 94.7%, 94.3% and 95.4%, respectively. Therefore, the irreversible capacities in these electrolyte solutions are approximately 5%, and smaller than those of graphite negative electrode in EC/EMC electrolyte solution [10]. The irreversible capacities may originate from the structural change of $LiCoO_2$ and/or the formation of SEI. The above-mentioned result also suggests that the amount (thickness) of SEI formed on $LiCoO_2$ electrode in the first cycle charge is very small (thin) if the irreversible capacity is consumed by the formation of SEI. Itagaki et al. [24] reported that the irreversible capacity of negative electrode in EC/EMC with 1 wt% ES was 35% and this large irreversible capacity originated by the formation of thick SEI film on graphite electrode. Contrary to the graphite electrode, the significant influence of ES on the $LiCoO_2$ was not observed in the results in Fig. 3.

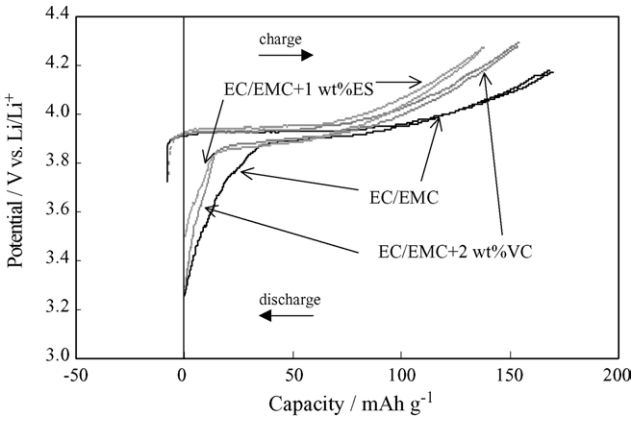


Fig. 3. Potential–capacity curves of the $LiCoO_2$ electrode in EC/EMC (solid line), EC/EMC + 2 wt% VC (dotted line) and EC/EMC + 1 wt% ES (dashed line) in the first cycle. The dc current density is 0.2 mA $cm^{-2}$.

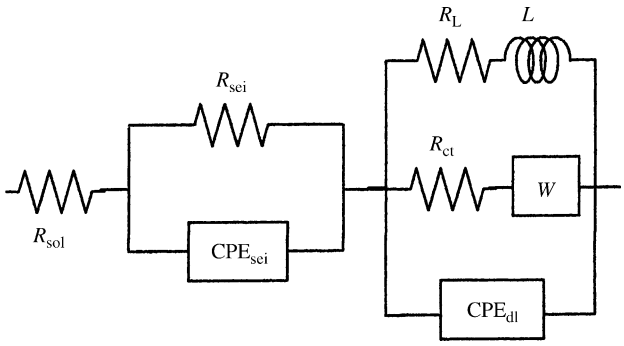


Fig. 4. The equivalent circuit for the $LiCoO_2$ electrode.

### 3.3. Discussion on the parameters determined by in situ EIS

The equivalent circuit for $LiCoO_2$ electrode in EC/EMC electrolyte is depicted in Fig. 4. In Fig. 4, $R_{sol}$ is the solution resistance, $R_{SEI}$ is the resistance of $Li^+$ permeation in SEI (the SEI resistance), $R_{ct}$ is charge transfer resistance on $LiCoO_2$. $CPE_{SEI}$ and $CPE_{dl}$ are constant phase elements (CPE) correspond to SEI capacitance at high frequency loop and electric double layer capacitance at low frequency loop, respectively. The CPE is an electric element to represent the shape of depressed capacitive loop, and it could be considered that the capacitance dispersion is due to the electrode roughness, the current and potential distributions and the porous structure [26,27]. The impedance of CPE, $Z_{CPE}$, is expressed by Eq. (1):

$$Z_{CPE} = \frac{1}{(j\omega)^{\alpha} Q} \tag{1}$$

where $Q$ is the CPE constant and $\alpha$ is the CPE exponent. Ue [25] stated that thin film was formed on positive electrode of LIRB and should be called as SEI. This film suppresses $CO_2$ gas evolution on the positive electrode [25]. Ue [25] analyzed SEI film on $LiCoO_2$ electrode in EC/EMC with $LiPF_6$ by ion chromatography, and reported that this film involved Li, F and $CO_3$. According to this report, the time constant for SEI film is arranged in the series with the time constant for the charge transfer in this equivalent circuit. Beside, Fig. 4 involves the inductance $L$ because the small inductive loop was observed in the impedance presented in Fig. 2. Moreover, $W$ is the diffusion Warburg impedance. Fig. 5 shows the typical impedance fitted using the equivalent circuit in Fig. 4 by Zview software (Solartron). The square symbols denote the experimental results of the instantaneous impedance and the curves represent the fitted results. The results involved the fitting errors within a few percents. When the impedance describes the negative resistance, the curve-fitting was performed for the experimental data except for the part of negative resistance loop.

Fig. 6 shows the plots of $R_{SEI}$ and $R_{ct}$, which are determined from the instantaneous impedance by the curve-fitting with the equivalent circuit presented in Fig. 4, against the capacity in the first cycle charge and discharge. In this section, the data in EC/EMC electrolyte solution is focused among the

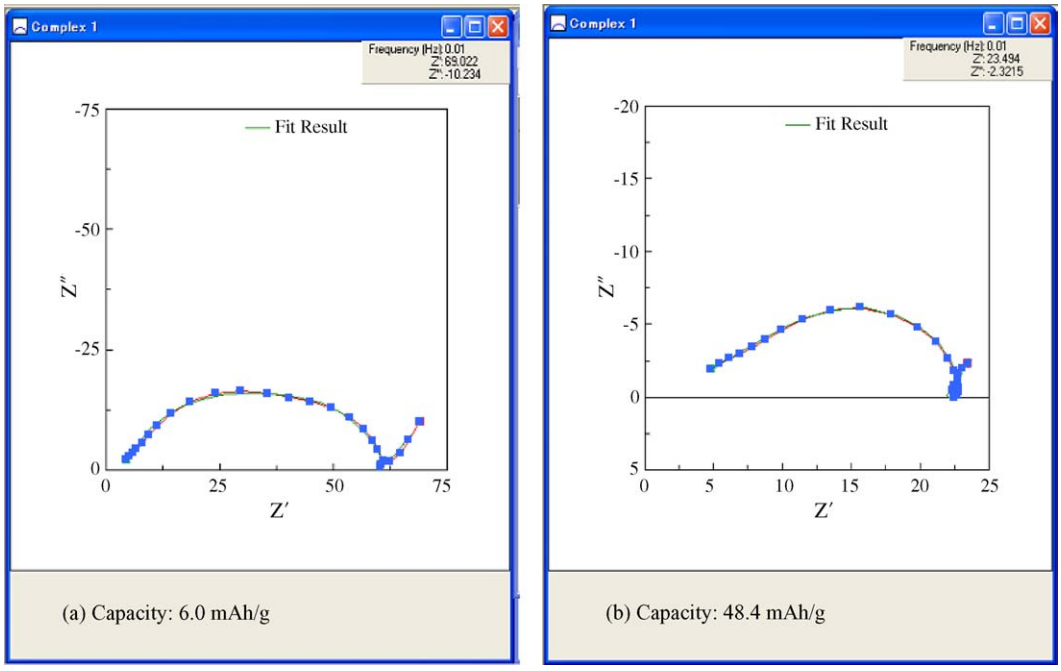


Fig. 5. Typical results fitted using the equivalent circuit in Fig. 4 by Zview software. The solid symbols denote the experimental results of instantaneous impedance at (a) 6.0 mAh $g^{-1}$ and (b) 48.4 mAh $g^{-1}$ in Fig. 2. The curve represents the fitted results.

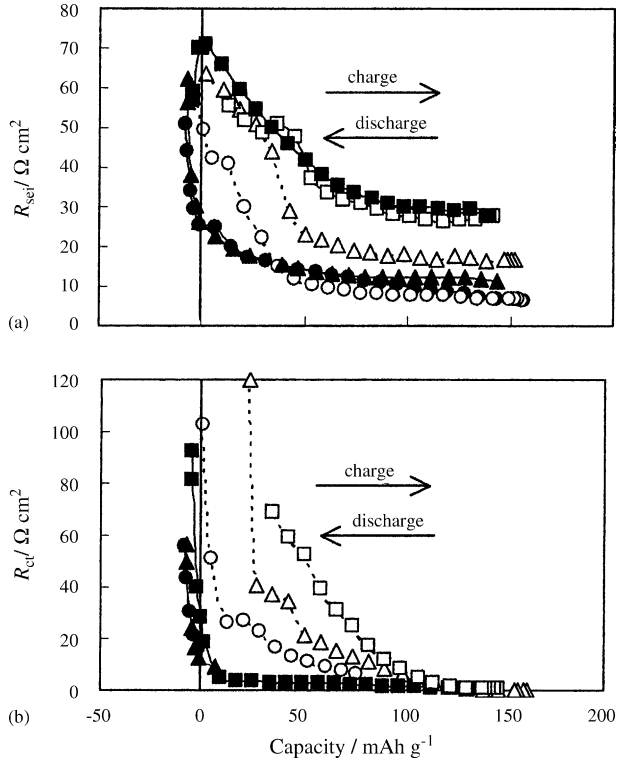


Fig. 6. The plots of (a) $R_{SEI}$ and (b) $R_{ct}$ of $LiCoO_2$ electrode against the capacity during the first charge–discharge cycle. Electrolyte solutions were 1 mol dm$^{-3}$ LiPFe–EC/EMC (3:7 by volume) ((●) during charge, (◯) during discharge), EC/EMC + 2 wt% VC ((▲) during charge, (△) during discharge) and EC/EMC + 1 wt% ES ((■) during charge, (□) during discharge).

various electrolyte solutions. In Fig. 6(a), the $R_{SEI}$ (symbol ●) takes 60 Ω cm$^2$ at the initial period and decreases to the constant value of 20 Ω cm$^2$ during the charge. Consequently, in the discharge, the $R_{SEI}$ (symbol ◯) stays at the almost same value as that at the end of charge, and increases until the approximately initial value in the charge. Zhang et al. [7] measured the electrochemical impedance of the $LiNiO_2$ positive electrode at OCV conditions, and reported that the reversible variations of $R_{SEI}$ during the charge and discharge sequence. Furthermore, they [7] observed the remarkable decrease of $R_{SEI}$ in the potential range of 3.4–3.8 V during the charge, and explained it by the significant increase in the ionic conductivity of SEI film. In the case of $LiCoO_2$ positive electrode in EC/EMC, the SEI structure is formed during the initial period and the $R_{SEI}$ decreases due to the increase of the ionic conductivity in the SEI film. Beside Itagaki et al. [10] reported that the $R_{SEI}$ of graphite negative electrode in EC/EMC showed the large hysteresis in charge–discharge sequence, where the $R_{SEI}$ in the discharge took smaller value than that in the charge. Furthermore, it's well known that the SEI film was formed on graphite electrode in EC/EMC during the first charge and maintained after the first cycle charge. It is considered that the reversible process of SEI structure on $LiCoO_2$ electrode is apparently different from the film formation on graphite negative electrode. The reversible process of $R_{SEI}$ may originate from that the SEI formation takes place by the reversible reaction on the $LiCoO_2$ electrode or that the conductivity of Li-ion in the SEI film is the function of the electrode potential.

In Fig. 6(b), the value of $R_{ct}$ (symbol ●) decreases abruptly at the initial period and decreases gradually later during the charge. During the discharge, the value of $R_{ct}$ (symbol ◯) increases with the small hysteresis. The electrode potential shifts toward noble at the initial period in the charge curve presented in Fig. 4. Therefore, the anodic reaction (deintercalation) rate increases and $R_{ct}$ decreases with the charge. The impedance analyses for LIRB except for references [10] and [24] were performed by ex situ measurement. In the case of ex situ EIS, the reciprocal of $R_{ct}$ is in proportion to the exchange current of intercalation and deintercalation of Li because the measurement is carried out under the equilibrium state. Contrary to this, since the intercalation or deintercalation rate is modulated electrochemically in the case of in situ EIS, the separate $R_{ct}$ for intercalation or deintercalation can be obtained. Beside, the diffusion of Li in the oxide particles is concerned with the intercalation and deintercalation. As the concentration profile of Li in oxide particles is not uniform during the measurement of in situ impedance, the additional mathematical treatment is required for the further analysis on diffusion process of Li.

### 3.4. Roles of VC and ES on the parameters

Aurbach et al. [11] reported that the addition of VC into the electrolyte decreases the impedance of $LiMn_2O_4$ and $LiNiC_2$ positive electrodes. Beside, the influence of ES has been investigated by various analytical methods as the SEI forming additive for the graphite negative electrode [12–14]. However, the effects of VC and ES on the surfaces of positive electrode are still unclear. In the present paper, the electrochemical impedance of $LiCoO_2$ electrode in EC/EMC with 2 wt% VC or 1 wt% ES was measured with the charge and discharge curves.

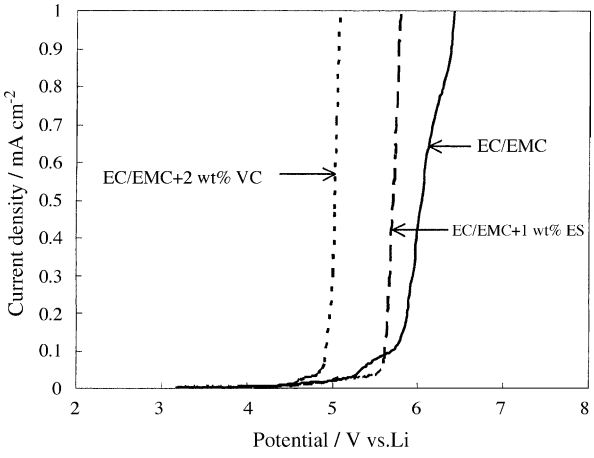


Fig. 7. Anodic polarization curves of the Pt electrode in EC/EMC (solid line), EC/EMC + 2 wt% VC (dotted line) and EC/EMC + 1 wt% ES (dashed line).

Fig. 7 shows the anodic polarization curves of Pt wire in three kinds of electrolyte solutions. In the EC/EMC electrolyte, the anodic current increases abruptly above approximately 5.2 V versus Li. This anodic current originated by the decomposition of the electrolyte solution. The potential of the current increase in EC/EMC with VC is much less noble than that in EC/EMC, suggesting that the VC is oxidized in EC/EMC above 4.5 V versus Li. In EC/EMC containing 1 wt% ES, the decomposition potential of the electrolyte is slightly less noble than that in EC/EMC. These results indicate that the ES is also oxidized in EC/EMC but the oxidation potential is nobler than that of VC.

Fig. 6 shows the relation between the capacity and the resistances ($R_{SEI}$ and $R_{ct}$) determined from the electrochemical impedance during charge and discharge sequence. The remarkable influences of VC and ES on $R_{ct}$ are not shown in the charge in Fig. 6(b). Beside, the additions of VC and ES increase the $R_{ct}$ in the discharge. In Fig. 6(a), the sequence of $R_{SEI}$ in EC/EMC with VC is almost same as that in EC/EMC, though the value of $R_{SEI}$ with VC takes a larger value than $R_{SEI}$ without VC during the discharge. This result indicates that the slight influence of VC on the electrochemical behavior of $LiCoO_2$ electrode in EC/EMC. On the other hand, $R_{SEI}$ in EC/EMC with ES takes significantly larger value than that in EC/EMC. The $R_{SEI}$ takes 65 $\Omega\,cm^2$ at the initial period and decreases gradually during the charge in the presence of ES. At the deep capacity above 100 mAh $g^{-1}$ the value of $R_{SEI}$ in the presence of ES is three times larger than that in EC/EMC. It is considered that the thick or low-conductive SEI film may be formed during the deintercalation of $LiCoO_2$ electrode in the presence of ES.

## 4. Summary

The electrochemical behavior of $LiCoO_2$ electrode in EC/EMC electrolyte was investigated by in situ EIS. By using in situ EIS, the separate charge transfer and film resistances for intercalation or deintercalation of Li can be obtained. The instantaneous impedance, which was determined by the cross-section of 3D impedance, showed two capacitive loops on the complex plane, and the high frequency loop was related to the resistance and the capacitance of SEI. The SEI resistance decreased and increased during the charge and discharge cycle, respectively. It was considered that the SEI structure was formed at the initial period of the charge and the SEI resistance varied by the reversible process. The addition of ES into EC/EMC electrolyte increased the SEI resistance, indicating that the thick or low-conductive SEI film is formed in the presence of ES.

## References

[1] E. Peled, J. Electrochem. Soc. 126 (1979) 2047.
[2] R. Yazami, D. Guerard, J. Power Sources 43/44 (1993) 39.
[3] J.O. Besenhard, M. Winter, J. Yang, W. Biberacher, J. Power Sources 54 (1995) 228.
[4] D. Aurbach, M.D. Levi, E. Levi, H. Teller, B. Markovsky, G. Salitra, J. Electrochem. Soc. 145 (1998) 3024.
[5] D. Aurbach, K. Gamolsky, B. Markovsky, G. Salitra, Y. Gefer, U. Heider, R. Oesten, M. Schmidt, J. Electrochem. Soc. 147 (2000) 1322.
[6] D. Ostrovskii, F. Ronci, B. Scrosati, P. Jacobsson, J. Power Sources 94 (2001) 183.
[7] S.S. Zhang, K. Xu, T.R. Jow, Electrochem. Solid-State Lett. 5 (2002) A92.
[8] S.-Ki. Jeong, M. Inaba, R. Mogi, Y. Iriyama, T. Abe, Z. Ogumi, Langmuir 17 (2001) 8281.
[9] M. Inaba, R. Mogi, S.-Ki. Jeong, Y. Iriyama, T. Abe, Z. Ogumi, Electrochem. Soc. Proc. 21 (2001) 521.
[10] M. Itagaki, N. Kobari, S. Yotsuda, K. Watanabe, S. Kinoshita, M. Ue, J. Power Sources 135 (2004) 255.
[11] D. Aurbach, K. Gamolsky, B. Markovsky, Y. Gofer, M. Schmidt, U. Heider, Electrochem. Acta 47 (2002) 1423.
[12] O. Matsuoka, A. Hiwara, T. Omi, M. Toriida, T. Hayashi, C. Tanaka, Y. Saito, T. Ishida, H. Tan, S.S. Ono, S. Yamamoto, J. Power Sources 108 (2002) 128.
[13] G.H. Wrodnigg, J.O. Besenhard, M. Winter, J. Electrochem. Soc. 146 (1999) 470.
[14] H. Ota, T. Akai, H. Namita, S. Yamaguchi, M. Nomura, J. Power Sources 119–121 (2003) 567.
[15] M. Itagaki, A. Taya, K. Watanabe, Electrochemistry 68 (2000) 596.
[16] T. Osaka, T. Momma, T. Tajima, Denki Kagaku 62 (1994) 350.
[17] Z. Stoynov, B. Savova-Stoynov, J. Electroanal. Chem. 183 (1985) 13.
[18] Z. Stoynov, B. Savova-Stoynov, T. Kossev, J. Power Sources 30 (1990) 275.
[19] N. Imanishi, M. Fuji, A. Hirano, Y. Takeda, M. Inaba, Z. Ogumi, Solid State Ionics 45–53 (2001) 140.
[20] C.K. Lee, K-I. Rhee, J. Power Sources 109 (2002) 17.
[21] E.-D. Jeong, M.-S. Won, Y.-B. Shim, J. Power Sources 70 (1998) 70.
[22] G.T.-K. Fey, W.-H. Yo, Y.-C. Chang, J. Power Sources 105 (2002) 82.
[23] X. Wu, S.B. Kim, J. Power Sources 109 (2002) 53.
[24] M. Itagaki, S. Yotsuda, N. Kobari, K. Watanabe, S. Kinoshita, M. Ue, Electrochim. Acta, in press.
[25] M. Ue, 206th Meeting of The Electrochemical Society, October (2004) (abstract 308).
[26] T. Pajkossy, J. Electroanal. Chem. 364 (1994) 111.
[27] P. Zoltowski, J. Electroanal. Chem. 443 (1998) 149.